REMOTE SOUNDING OF THE CIRRUS OPTICAL DEPTH AND TEMPERATURE FROM 3.7 AND 11 MICROMETER WINDOWS

Huang Runheng (黄润恒)

Institute of Atmospheric Physics, Academia Sinica, Beijing

and Kuo-Nan Liou (廖国男)

Department of Meteorology, University of Utah, Salt Lake City,Utah, U.S.A.

ABSTRACT

On the basis of forward IR radiation transfer analyses for an atmosphere containing semi-transparent, non-black cirrus, parameterization equations are derived for the retrieval of the cloud optical depth and cloud temperature utilizing AVHRR 3.7 and 10.8 μm channels. The retrieval techniques developed involve the use of either dual-frequency or dual-scanning angle radiance observations. We show that the cloud optical depth and cloud temperature may be inferred successively from the observed brightness temperature differences using these two techniques. Numerical experiments and error analyses demonstrate that the dual-frequency method is specifically appropriate for optically thin cirrus cases ($\tau < 1$). In case the optical depth of cirrus is close to 3, combination of dual-frequency and dual-scanning angle methods is shown to give reasonable accuracy for the cloud optical depth and temperature retrieval.

I. INTRODUCTION

In recent years, there has been increasing scientific effort in deriving new information on the cloud cover and vertical structure over a sufficiently long period of time from radiance measurements routinely provided by orbiting meteorological satellites. The urgent need for an updated and reliable cloud climatology has been well recognized in view of the fact that clouds,which constantly cover about 50% over the global sky, are the most important regulators of the radiation balance of the earth-atmosphere system. It is apparent that availability of a consistent and reliable cloud climatology data set could lead to further improvements in climate and weather prediction modelling.

Clouds composed of water droplets are generally optically thick because of high droplet concentrations, and therefore, it is physically appropriate to assume these clouds to be blackbodies in thermal infrared region. However, high level clouds, which contain a significant amount of large, nonspherical ice crystals having low concentrations, are normally optically thin and nonblack. It has been noted that cirrus has introduced serious difficulties in remote sensing of atmospheric temperature and humidity profiles as well as surface conditions. It is important, therefore to reliably determine the radiative characteristic and temperature structure of cirrus over the global scale in relation to the atmospheric profile and surface temperature determinations from infrared sounding channels. Moreover, the mapping of cirrus in terms of their spatial coverage and vertical ice content (or equivalently, their optical depth) over the globe routinely would be of vital significance in conjunction with climate studies and numerical weather prediction.

Following previous retrieval analyses proposed by Liou [1] ,Feddes and Liou [2] ,Liou et al.[3] and Yeh and Liou[4] utilizing various combinations of thermal infrared channels we wish to present in this paper new techniques for the determination of the cirrus optical depth and temperature utilizing

NOAA 7 AVHRR channels. Section II contains a brief description of the characteristics of the AVHRR infrared channels and the fundamental procedure for the calculation of infrared radiances in cirrus cloudy atmospheres. Section III discusses radiative transfer parameterizations for applications to the retrieval of the cloud optical depth, cloud temperature and clear-air brightness temperature. Two approaches are developed. These include the use of two channels (3.7 and 10.8μm) and two scanning angles from either channel. In Section IV we present numerical experiments and error analyses in conjunction with these two retrieval techniques along with their practicalities and limitations when cirrus is involved. Finally, conclusions are given in Section V.

II. FORWARD COMPUTATIONAL PROCEDURES

The advanced very high resolution radiometer (AVHRR) aboard the NOAA 7 Satellite has three channels located at the 3.7 (channel 3), 10.8 (channel 4) and 11.9 (channel 5) μm window regions. Each channel having a finite bandwidth is divided into several subintervals with widths of 20 and 30 cm^{-1} for 3.7 μm and 10.8-11.9 μm, respectively (Weinreb and Hill[5]). For each subinterval, upwelling radiances $R_a^{\uparrow}(z_b)$ reaching the cloud base and downward radiances $R_a^{\downarrow}(z_t)$ at the cloud top can be computed from the clear-air radiative transfer program as depicted in Fig. 1, where z_b and z_t are cloud base and top heights, respectively.
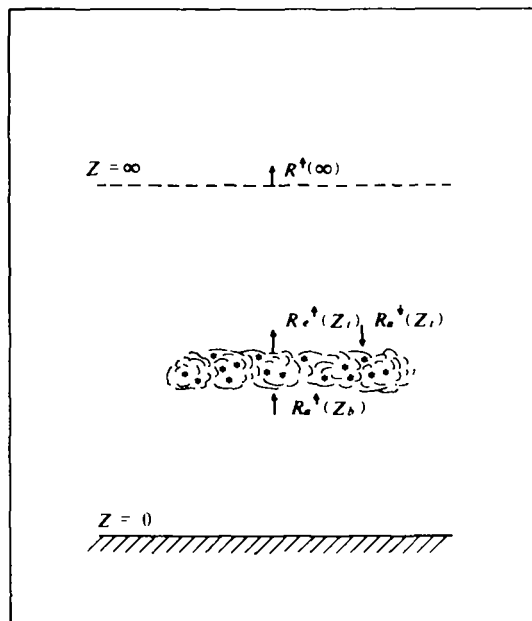

Fig. 1. Configuration of the transfer of IR radiation through a cloud.

The radiative transfer equation of a plane-parallel cloudy atmosphere is first solved by using the discrete-ordinates method with $R_a(z_t)$ and $R_a(z_b)$ as boundary conditions to give the upwelling radiance emergent from the cloud top $R_c(z_t)$ (Huang and Liou[6]). Subsequently, the upwelling radiance $R(\infty)$ at the top of the atmosphere is given by

$$R(\infty) = R_c^{\uparrow}(z_t)T_a(z_t,\infty) + R_a^{\uparrow}(z_t,\infty), \tag{1}$$

where $T_a(z_t,\infty)$ and $R_a^{\uparrow}(z,\infty)$ are the clear-air transmittance and upwelling radiance due only to the gaseous absorption and emission above the cloud top, respectively. The dependence of the surface

reflectivity, γ_i, on the wavenumber of the subinterval is taken into consideration in the calculation. Atmospheric absorption and emission above high cirrus can be neglected for the infrared window channels (Liou [17]). Thus, $T_a(z_t, \infty) = 1$, and $R_a(z_t, \infty) = 0$ so that $R(\infty) \approx R_c(z_t)$. After obtaining each subinterval radiance, the radiance for each channel is computed by

$$\bar{R} = \sum_i R_i w_i \bigg/ \sum_i w_i, \tag{2}$$

where w_i is the spectral response weight of the instrument in the ith subinterval.

Table 1. Central Wavenumbers, Spectral Responses and Surface Reflectivities for the Subintervals of Three AVHRR Channels

i	v_i (cm^{-1})	w_i			γ_i
		Channel 3	Channel 4	Channel 5	
1	775			0	0.0228
2	805			0.42	0.0159
3	835		0	0.89	0.0114
4	865		0.02	0.75	0.0086
5	895		0.661	0.03	0.0080
6	925		0.917	0	0.0081
7	955		0.985		0.0088
8	985		0.010		0.0097
9	2450	0.002			0.0218
10	2470	0.009			0.0219
11	2490	0.020			0.0220
12	2510	0.080			0.0221
13	2530	0.334			0.0223
14	2550	0.748			0.0225
15	2570	0.902			0.0227
16	2590	0.939			0.0229
17	2610	0.966			0.0232
18	2630	0.943			0.0236
19	2650	0.928			0.0240
20	2670	0.976			0.0244
21	2690	0.981			0.0248
22	2710	0.996			0.0252
23	2730	0.997			0.0256
24	2750	0.983			0.0260
25	2770	0.966			0.0264
26	2790	0.944			0.0268
27	2810	0.850			0.0272
28	2830	0.522			0.0276
29	2850	0.186			0.0280
30	2870	0.053			0.0284
31	2890	0.010			0.0288

Shown in Table 1 are the central wavenumber, spectral response and surface reflectivity of each subinterval for the NOAA 7 AVHRR at two infrared window regions (McClain, 1983, private communication). It can be seen in Table 1 that the spectral response of each channel has a very sharp

cut-off. For the purpose of economizing the computational effort, we use only 13—28, 5—7 and 2—4 subintervals to represent channels 3,4 and 5, respectively.

In the following analysis, an atmospheric profile for 30° N, July is employed which is denoted as"standard profile." A homogeneous and isothermal cirrus is superimposed onto the profile using a cloud height and thickness of 8.3 and 1.7 km, respectively. In order to examine the relationship between the radiative properties of cirrus and the atomspheric profile, pseudo-random numbers uniformly distributed in an interval (-a,a) are added to the standard temperature and humidity profile. These are (-5,5 K) and (-10,10%) for the temperature and humidity, respectively. The profile so obtained is called the random profile. 40 sets of random profiles were used in this study. Again, a homogeneous and isothermal cirrus of the same height and thickness is superimposed onto the random profiles. The cloud temperature is simply taken to be an average of the environmental temperatures of the cloud top and base, while the surface temperature is assumed to be the temperature at the 1000 mb level with a value of 293.6 K for the standard profile.

Based on the comprehensive observations of Weickmann[8] and Heymsfield[9], cirrus contains primarily hexagonal columns whose major axes vary from 100 to 500 μm. In reference to the size distribution observed by Heymsfield, we assume for the purpose of light scattering calculations that ice columns are randomly oriented in space, having a mean length and width of 300 and 120 μm, respectively. Using the ray-tracing technique developed by Cai and Liou[10], light scattering calculations for hexagonal ice columns for three infrared wavelengths are carried out. Table 2 depicts the complex index of refraction of ice (Schaaf and Williams[11]) for these wavelengths and the calculated single scattering parameters.

Table 2. Real and Imaginary Parts of the Refractive Index, Scattering and Extinction Cross Sections and Single-Scattering Albedo for Three Infrared Wavelengths

λ (μm)	m_r	m_i	σ_s (10^{-4} cm^2)	σ_e (10^{-4} cm^2)	$\tilde{\omega}_o$
3.7	1.383	0.007	3.205	5.623	0.567
10.8	1.038	0.169	2.997	5.653	0.530
11.9	1.259	0.409	3.110	5.653	0.550

In Fig. 2 are shown the scattering phase functions for randomly oriented ice columns for 3.7 and 10.8 μm wavelengths. A common feature in these patterns is a very sharp forward scattering peak, which is much stronger for 3.7 μm than for 10.8 μm. The phase function for the 3.7 μm wavelength reveals two maximum features at the 22 and 46° halo positions which, however, are not shown for the 10.8 μm because of large absorption of ice at this wavelength. Note that the phase function pattern for the 11.9 μm wavelength is very similar to that for the 10.8 μm wavelength. In order to take into account the effect of the strong forward scattering on radiative transfer, 64 streams are employed to represent the azimuthally averaged phase function so that the normalization condition

$$\frac{1}{2}\int_{-1}^{1} \bar{p}(\mu,\mu')d\mu = 1$$

is satisfied. Since the complex index of refraction for ice does not vary significantly in a narrow range of wavelength, it suffices to use single scattering parameters of the central wavelength of each channel for all the subintervals. Consequently, the radiative transfer equation needs to be solved only once for each channel.

Weinreb and Hill[5] suggest that the total transmittance of the molecular atmosphere in rectangular subintervals is a product of the individual transmittances which are attributed to various absorption mechanisms. For the 11—12 μm window, they are due to the water vapor spectral line, water vapor self-broadened continuum and uniformly mixed gases, mainly carbon dioxide. Thus, the total transmittance $T_v = T_l\,T_{sb}\,T_u$, where T_l, T_{sb} and T_u denote, respectively, the transmittances attributed to the aforementioned absorption mechanisms. For the 3.7 μm window, the major absorbing gases are water vapor and uniformly mixed gases (CO_2, N_2O and CH_4) as well as molecular nitrogen. In this region, the water vapor self-broadened continuum can be neglected, but the water vapor foreign-broadened continuum should be taken into account. Thus, $T_v(z) = T_l\,T_f\,T_N\,T_u$, where T_f and T_N represent transmittances due to the water vapor foreign-broadened continuum and molecular nitrogen, respectively. Moreover, we apply the look-up tables proposed by Weinreb and Hill[5] to convert the calculated radiance to the equivalent brightness temperature. One of the advantages of this procedure is that the look-up tables have taken into consideration the spectral response properties so that the error is less than that produced by conversion using a central reference wavenumber.

Because of the absorption by atmospheric molecules, the brightness temperature observed at the satellite point under the clear-air condition is smaller than the surface temperature. The difference between them is defined as "atmospheric attenuation" denoted by

$$\Delta a = T_s - TB_a, \tag{3}$$

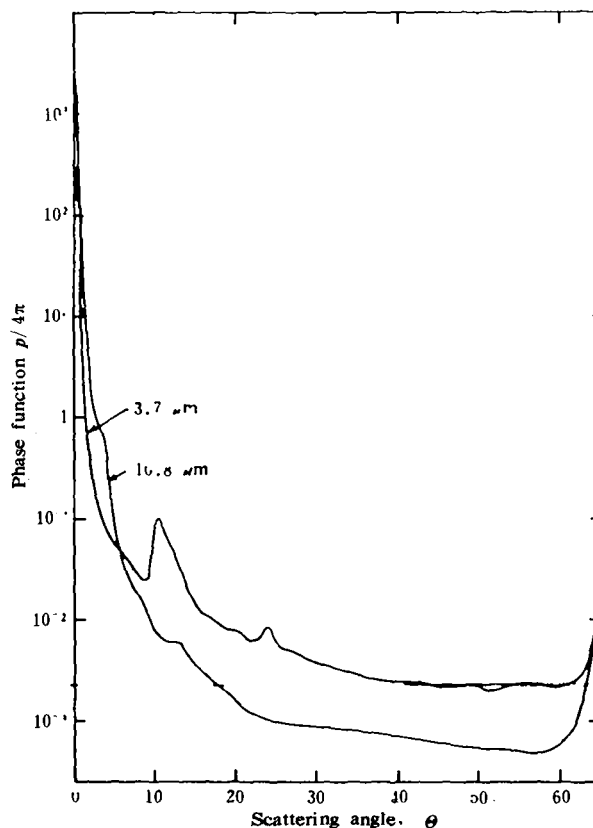where TB_a is the brightness temperature corresponding to the clear-air column radiance. In general, it

Fig. 2. The scattering phase function of hexagonal ice crystals randomly oriented in space with sizes of 300 μm in length and 120 μm in width for wavelengths of 3.7 and 10.8 μm.

depends not only on the total precipitable water but also on the surface temperature and atmospheric temperature profile. We ultilized the transmittance model mentioned previously to evaluate the clear-air radiative transfer problem at the IR windows. Shown in Fig. 3 is the atmospheric attenuation as a function of the total water vapor content for the standard temperature profile, but with different water vapor amounts. It is evident that the 3.7 μm channel is the most transparent among these window channels. We also note that the difference in the atmospheric attenuation between 3.7 μm and 10.8 μm channels is less than 0.5 K for a total precipitable water less than 10 g cm^{-2}.
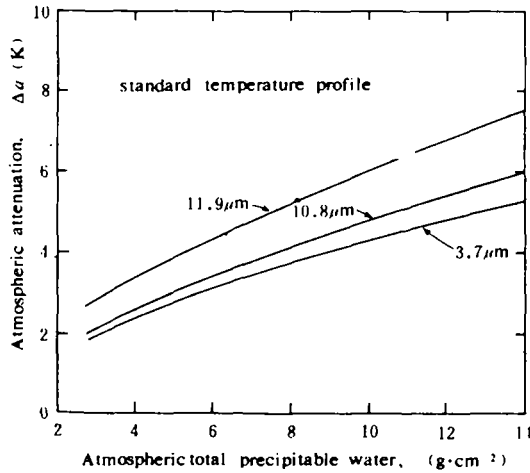
Fig. 3. The clear-air atmospheric attenuation for 3.7, 10.8 and 11.9 μm channels as a function of the total atmospheric precipitable water

Next, we define the intensity emissivity and transmissivity of the subinterval as follows:

$$\begin{aligned} \varepsilon_i(\mu) &= I_{1,i}(\mu)/B_i(T_c) \\ t_i(\mu) &= I_{2,i}(\mu)/R_{a,i}(\mu) \end{aligned} \Bigg\}, \tag{4}$$

where $I_{1,i}(\mu)$ denotes the upwelling radiance of the ith subinterval leaving the cloud top in the direction of μ, which is produced by the cloud emission only. $I_{2,i}(\mu)$ and $R_{ai}(\mu)$ are the upward radiances of the ith
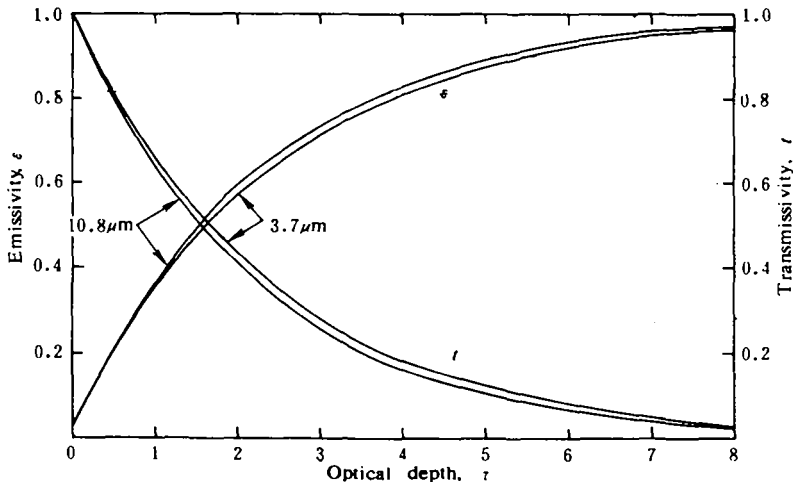
Fig. 4. The broadband intensity emissivity and transmissivity for cirrus as a function of the cloud optical depth.

subinterval leaving the cloud top and reaching the cloud base in the direction of μ, respectively, which are generated by the external radiation source. The advantage of separating the total intensity into I_1 and I_2 is that the transmissivity defined in Eq.(4) is a function of the cloud optical depth only, and is independent of the cloud temperature.

In accordance with the definition denoted in Eq. (2), the emissivity and transmissivity for each channel may be derived. Based on the resulting transfer calculation, we find that radiative characteristics of cirrus at the 11.9 μm channel are very close to those at the 10.8 μm channel. Depicted in Fig. 4 is the upwelling emissivity and transmissivity ($\mu = 1$) as a function of the optical depth for 3.7 and 10.8 μm channels. It can be seen that the transmissivity for the 3.7 μm channel is higher than that of 10.8 μm. This is due to the stronger forward scattering of ice crystals for the shorter wavelength. From a series of numerical calculations we also find that the reflectivity of cirrus generated by the external radiation source is much smaller than the transmissivity. For an optical depth less than about 10, we may safely assume that $\varepsilon(\mu) = 1 - t(\mu)$.

Finally, from the look-up tables, we may obtain the brightness temperature, TB_c, corresponding to the radiance emergent from the cloud top. The difference between TB_a and TB_c is defined as "the cloud attenuation" in the form

$$\Delta c = TB_a - TB_c . \tag{5}$$

In general, Δc depends on the cloud optical depth and cloud temperature as well as the emergent direction.

III. PARAMETERIZATION OF RADIATIVE TRANSFER EQUATION FOR RETRIEVAL ANALYSIS

In reference to Fig. 1 and Eq. 4, which define the cloud emissivity and transmissivity, the radiance emergent from the cloud top can be expressed by

$$R_c(\theta) = R_a(\theta)t(\theta) + \varepsilon(\theta)B(T_c). \tag{6}$$

Moreover, through Eqs. (3) and (5) the corresponding brightness temperature is given by

$$TB_c = T_s - \Delta a - \Delta c, \tag{7}$$

where Δa and Δc are, respectively, the atmospheric and cloud attenuations defined in the previous section. In this manner the cloud effect is separated from the underlying clear atmosphere. Based on the forward radiative transfer analysis, ε and t are found to be monotonic functions of the cloud optical depth. Thus, the radiance at the atmospheric top or approximately the cloud top will depend on the radiance reaching the cloud base, cloud optical depth and cloud temperature. All these quantities are important from the point of view of remote sounding.

An inspection of Fig. 4 reveals that $t(\theta)$ and $\varepsilon(\theta)$ may be expressed by a polynomial of $\tau \leqslant 3$ as follows:

$$\left.\begin{matrix} t(\theta) \\ \varepsilon(\theta) \end{matrix}\right\} = a + b\tau + c\tau^2 . \tag{8}$$

Depicted in Table 3 are empirical coefficients and RMS regression errors for the cloud emissivity at 3.7 and 10.8 μm wavelengths for two emergent directions. These values are derived from results of theoretical transfer calculations. Below, we present two techniques for the reconstruction of the cloud parameters by using the "observed" radiances.

(1) *Multi-channel*

As illustrated in Fig. 3, the atmospheric attenuation of 3.7 μm and 10.8 μm channels is

Table 3. Empirical Coefficients for the Cloud Emissivity as a Function of the Cloud Optical Depth for 3.7 and 10.8 μm Channels

θ(°)	λ(μm)	a	b	c	RMS
0	3.7	0.0077	0.3797	−0.0485	0.0033
	10.8	0.0090	0.4033	−0.0533	0.0038
35.6	3.7	0.0273	0.4442	−0.0631	0.0053
	10.8	0.0280	0.4494	−0.0644	0.0005

approximately the same. But the cloud attenuation of these two channels differs significantly. Thus, we apply Eq. (7) for channels 3 and 4 when $\mu = 1$ (or $\theta = 0$) to eliminate the surface and atmospheric effects. Subtracting one from the other leads to

$$TB_3(0) - TB_4(0) = \Delta c_4(0) - \Delta c_3(0),\tag{9}$$

where $\Delta c_4 - \Delta c_3$ denotes the cloud attenuation difference between the two channels which depends mainly on the optical depth and for simplicity we let $TB_{c_{3,4}} = TB_{3,4}$. In Fig. 5, values of $(TB_3 - TB_4)$ are shown as a function of the optical depth. The dark circles in the figure represent mean values of the brightness temperature differences for 41 profiles (one standard profile and 40 random profiles), while the vertical bar denotes the standard deviation. The upper solid curve represents the best fitting for results corresponding to optical depths less than three, employing a second order polynomial fitting in the optical depth denoted in Eq. (8). Table 4 lists the regression coefficients and RMS errors for the brightness temperature difference using the dual-frequency and dual-scanning angle techniques.

Table 4. Regression Coefficients for Brightness Temperature Differences ΔT Involving Dual-Frequency and Dual-Scanning Angle Techniques

ΔT	a	b	c	RMS(K)
$TB_3(0) - TB_4(0)$	0.2878	8.9302	−1.4601	0.91
$TB_3(0) - TB_3(\theta)$	0.2390	2.5157	−0.2251	0.13

After the optical depth has been estimated we then utilize Eq. (6) for channels 3 and 4 to retrieve the cloud temperature. We write

$$\left.\begin{array}{l} R_3 = R_{a,3}(1 - \varepsilon_3) + \varepsilon_3 B_3(T_c) \\ R_4 = R_{a,4}(1 - \varepsilon_4) + \varepsilon_4 B_4(T_c) \end{array}\right\}.\tag{10}$$

In these equations ε_3 and ε_4 may be calculated from Eq. (8) using the optical depth determined from Fig. 5. In order to eliminate R_a and $B(T_c)$ from Eq. (10), we utilize the statistical relationships between the two channels for these values. From forward transfer calculations, we find that there are approximate linear relationships between clear-air radiances reaching the cloud base for 3.7 and 10.8 μm channels such that $R_{a,4} = a_1 + b_1 R_{a,3}$. Also, $B_3 \approx a_2 + b_2 B_4$ where a_1, a_2 and b_1, b_2 are constants. Hence, once R_3 and R_4 have been given from the measured radiances, $R_{a,3}$ (or $R_{a,4}$) and the cloud temperature via B_3 (or B_4) may be estimated from Eq. (10) simultaneously. In these analyses, two

measurements give three unknown variables through a number of statistical relationships. Note that $R_{a,3}$ (or $R_{a,4}$) is an intermediate parameterization variable for the purpose of retrieving τ and T_c from R_3 and R_4.

(2) Multi-scanning angle

Transfer calculations for clear atmospheres show that the clear column attenuation difference between two emergent angles is negligibly small if the angular deviations are less than 50°. Thus, by utilizing Eq. (7) for two scanning angles using one channel, the surface and atmospheric effects may be removed so that

$$TB_c(0^\circ) - TB_c(\theta) = \Delta c(\theta) - \Delta c(0^\circ). \tag{11}$$

In Fig. 5 the cloud attenuation difference is shown for the zenith and a scanning angle of 35.6° using $3.7 \ \mu m$ and $10.8 \ \mu m$ (dashed curve) channels. It can be seen that the response range of the cloud attenuation difference to the optical depth is much larger for the $3.7 \ \mu m$ channel than for the $10.8 \ \mu m$ channel. In a manner similar to the multi-channel method, we express Eq. (11) in terms of the second order polynomial of the optical depth with the unknown coefficients determined from the statistical regression analysis. In Table 4 are listed the regression coefficients and RMS errors for the brightness temperature difference employing the multi-scanning angle technique.

As in the dual-frequency method, the optical depth may be estimated by using the empirical relationship between the cloud attenuation difference and the optical depth. Then, the emissivities in two directions can be calculated from Eq. (8). Substituting $\varepsilon(\theta)$ into the radiance parameterization equation denoted in Eq. (6) for two emergent angles, we have

$$R_c(0^\circ) = R_a(0^\circ)[1 - \varepsilon(0^\circ)] + \varepsilon(0^\circ)B(T_c),$$
$$R_c(\theta) = R_a(\theta)[1 - \varepsilon(\theta)] + \varepsilon(\theta)B(T_c). \tag{12}$$

Since $R_a(0^\circ) \approx R_a(\theta)$, it follows that the clear-air radiance R_a and blackbody radiance $B(T_c)$ may be derived analytically from two measurements $R_c(0^\circ)$ and $R_c(\theta)$.

As mentioned above, the cloud attenuation depends in some degree on the cloud temperature. The use of the cloud attenuation difference technique, either in the form of $TB_3(0) - TB_4(0)$ or $TB_3(0) - TB_3(\theta)$, can only remove the cloud temperature effect partly. The vertical bar in Fig. 5 indicates the uncertainty of the brightness temperature difference as a function of the optical depth, resulting from variations of the atmospheric temperature and humidity profiles. The uncertainty appears to increase with increasing optical depths. Therefore, the reconstruction of the optical depth by using either multi-channel or multi-scanning angle method is subject to error and error analyses are required in the hypothetical retrieval experiment. The following section is concerned with the error analysis.

IV. NUMERICAL EXPERIMENTS AND ERROR ANALYSES

Based on the retrieval techniques outlined in the preceding section, the necessary observations are $R_3(0^0)$, $R_3(\theta)$, and $R_4(0^0)$. These quantities may in principle be determined from forward radiative transfer calculations involving cloudy atmospheres for the purpose of simulation studies. The look-up tables presented by Weinreb and Hill [5] are then used to convert the radiances to the equivalent brightness temperatures.

The optical depth may be directly obtained from the brightness temperature difference in dual-frequency or dual-scanning angle observations via Fig. 5. It is seen that the brightness temperature difference increases with increasing optical depth initially and decreases with further increase of the optical depth. We use a second order polynomial in the optical depth to represent the statistical relationship between the brightness temperature difference and the optical depth through Eqs. (7) and

(9). The ranges of optical depths, which are applicable in these experiments, are about 3 and 6 for multi-channel and multi-scanning techniques, respectively.

The intensity emissivity and transmissivity can be evaluated by substituting the reconstructed optical depth in Eq.(8). Then, using the known optical depth, the radiance reaching the cloud base and the cloud temperature can be simultaneously derived from Eq.(10) or (12). Employing the dual-scanning angle technique, we find that $\varepsilon(\theta)R(0) - \varepsilon(0)R(\theta) > 0$, and $\varepsilon(\theta)t(0) - \varepsilon(0)t(\theta) > 0$. These conditions assure that a positive solution of the radiance R_a can be obtained. However, the error in the retrieved optical depth may lead to the condition that $t(0) \ R(\theta) - t(\theta)R(0) < 0$, which may produce a negative radiance value. When this occurs, we artificially impose an additional constraint such as $t(0)/t(\theta) > R(0)/R(\theta)$ on Eq. (12). It turns out, however, that the constrained adjustment on $t(0)$, $t(\theta)$ has insignificant effects on the reconstructed radiance reaching the cloud base.

In order to examine the effect of the observed radiance error on the retrieval, we impose a series of pseudo-random numbers uniformly distributed in the interval $(-\sigma, \sigma)$ on the simulated radiances, where σ denotes the maximum percentage of random error. In the following numerical experiments we select optical depths of 0.5 and 3 to represent optically thin and moderate thick cirrus, respectively. The temperatures of cirrus are assumed to be 230, 235, and 240 K. The dual-frequency and dual-scanning angle techniques are simultaneously applied to reconstruct the optical depth, clear column brightness temperature and cloud temperature for 41 sets of cloudy atmospheric profiles. The average retrieval value and its standard deviation are displayed to indicate the significance of reconstructed results.
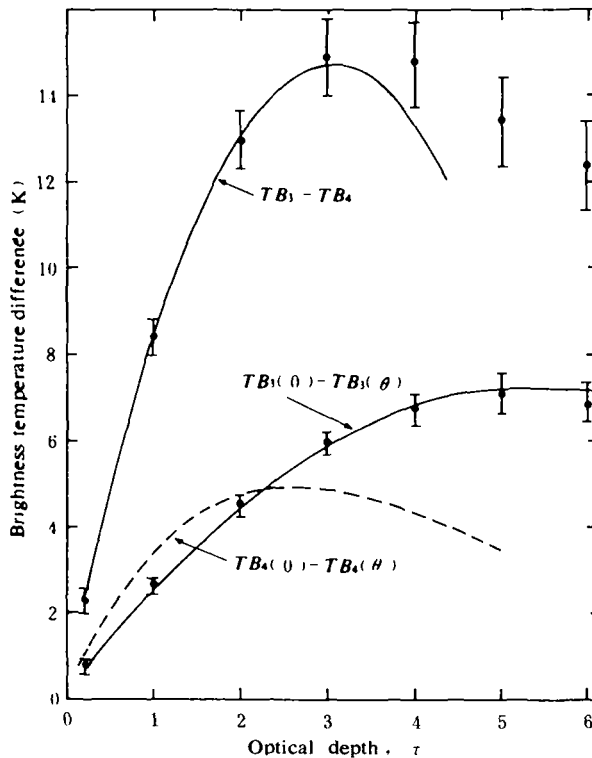

Fig. 5. The brightness temperature difference utilizing either dual-frequency or dual-scanning angle approach as a function of the cloud optical depth.

Fig. 6 shows the retrieval results involving a thin cirrus with a temperature of 230 K. The dark circle and solid curve shown in this figure represent the results using the dual-frequency technique,
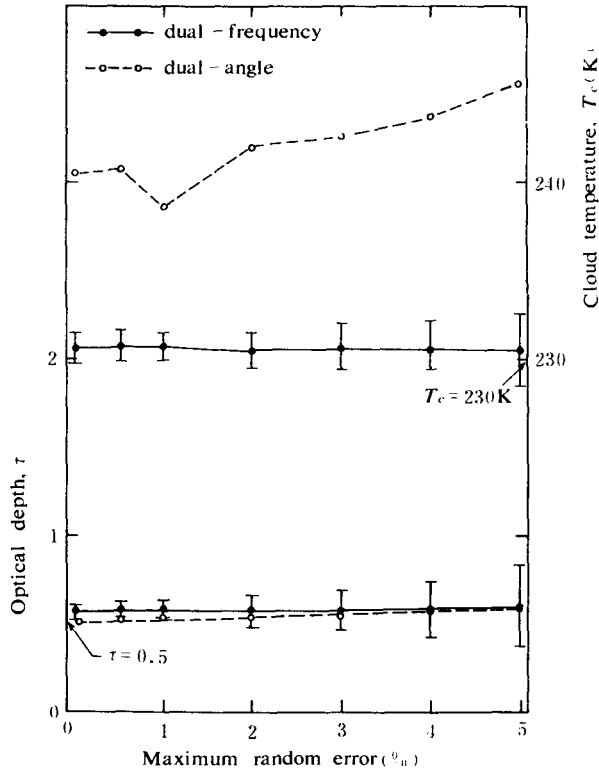
Fig. 6. Retrieval results of an optically thin cirrus with a cloud temperature of 230 K using either dual-frequency or dual-scanning angle techniques as a function of the maximum random error.

while the open circle and dashed curve correspond to those using the dual-angle technique. The vertical bar indicates the root mean square deviation about the average. It appears that these two retrieval techniques give reasonable optical depth values for an optically thin cirrus. The mean value depends weakly on the observed error and it is very close to the true value of 0.5, whereas the RMS deviation increases with increasing observed error. Fig. 6 also indicates that the dual-frequency technique can give an accurate cloud temperature. The difference between the retrieval mean and true cloud temperature (230K) is less than 1 K. Again, the RMS deviation depends on the observed error. For a maximum random error of 2%, the RMS deviation is 1 K. The cloud temperature retrieved from the dual-angle technique, on the other hand, is systematically larger than the true value. The possible reason is due to the fact that the atmospheric attenuation is assumed to be the same at two emergent directions. In addition, the look-up tables for the 3.7 μm channel have a very sharp variation in the temperature range of 200—240 K. A small change in the radiance can cause a large variation in the equivalent brightness temperature. For example, if there is an error of 0.01 erg sec^{-1} cm^{-2} cm in the reconstructed radiance, the corresponding variations are 6 and 1 K for temperatures of 230 and 280 K, respectively.

    Fig. 7 depicts retrieval results for a moderate thick cirrus with a cloud temperature of 235 K. It is evident that the reconstructed optical depth derived from the dual-angle technique is significantly better than that from the dual-frequency counterpart for maximum random errors less than about 3%. The dual-frequency technique underestimates the optical depth of a thick cirrus. This is because the brightness temperature difference between channels 3 and 4 approaches a maximum value as shown in Fig. 5. A small variation in the brightness temperature difference will result in a noticeable difference in

the retrieved optical depth. The curves in the upper part of Fig. 7 show that the reconstructed cloud temperature using the dual-scanning angle technique is slightly better than that using the dual-frequency technique. But both are systematically smaller than the true value. For a maximum random error of 2%, the deviation of reconstructed cloud temperature from the true value is 2.4 K. Both Figs. 6 and 7 also indicate that the standard deviation increases with increasing optical depths. The ratio of the standard deviation of the reconstructed optical depth to its average is nearly constant for optically thin and moderate thick cirrus cases. But for the reconstructed cloud temperature, this ratio for moderate thick cirrus is larger than that for thin cirrus. This implies that the retrieval accuracy of cloud temperature is less accurate than that for the optical depth.

Table 5.   RMS Deviations of the Retrieved Clear-Air Brightness Temperature for 41 Profiles in Units of K

Max.RMS(%)		0	.5	1	2	3	4	5
$\tau = 0.5$	(1)	0.5	.6	.7	1.0	1.4	1.9	2.3
	(2)	.5	.6	.9	1.7	2.4	3.3	4.0
$\tau = 3.0$	(1)	3.6	3.6	3.6	3.8	4.0	4.3	4.3
	(2)	1.2	1.1	1.1	1.6	2.3	3.8	4.9
$\tau = 3.0$	(1)+(2)	1.3	1.4	1.5	2.1	2.6	3.2	3.6

(1) and (2) denote, respectively, dual-frequency and dual-scanning angle techniques.

Because clear-column brightness temperatures are different from the 41 sets of cloudy atmospheric profiles, the accuracy of their retrieval results may best be measured by the root mean square difference between the reconstructed and true values. Shown in Table 5 are the RMS deviations for two retrieval techniques. This table lists the average of retrieval results for 41 cloudy profiles with same optical depth but with three different cloud temperatures. For an optically thin cirrus the RMS deviations of retrived clear-column brightness temperatures are 1 and 1.7 K using dual-frequency and dual-scanning angle techniques, respectively when the maximum random error is 2%. For an intermediate thick cirrus the retrieval accuracy using the dual-frequency technique decreases significantly. The RMS deviation is as much as 3.8 K. Under the same condition the RMS deviation for using the dual-scanning angle technique is only 1.6 K.

On the basis of the above analysis, it seems that when an optically moderate thick cirrus is involved the dual-angle is better than the dual-frequency technique. But as far as the temperature of a thick cirrus is concerned, neither the dual-angle technique nor the dual-frequency techniuqe can give satisfactory results. Taking advantage of the dual-angle technique in retrieving the optical depth, we present a combined technique utilizing both dual-frequency and dual-angle observations. Substituting the reconstructed optical depth derived from dual-angle observations in Eq. (9), the clear column brightness temperature and cloud temperature can be derived. Results of the combined method are shown in Fig. 8 and the last row of Table 5. It can be seen that the retrieval accuracy of the cloud temperature is improved noticeably. If maximum random error of 2% is incorporated in the analysis, the average deviations for cirrus with cloud temperatures of 230, 235 and 240 K are 0.2, 1 and 2 K, respectively. Also, the RMS deviation for the reconstructed clear-column brightness temperature is 2.1 K. It should be noted that the results of the combined technique involving an optically thin cirrus are nearly the same as those of the dual-frequency technique, since the optical depths derived from these

two techniques are similar. It seems that the dual-frequency technique has a better retrieval result when optically thin cirri are present, whereas the combined retrieval technique can improve the retrieval accuracy when optically thick cirri are involved.
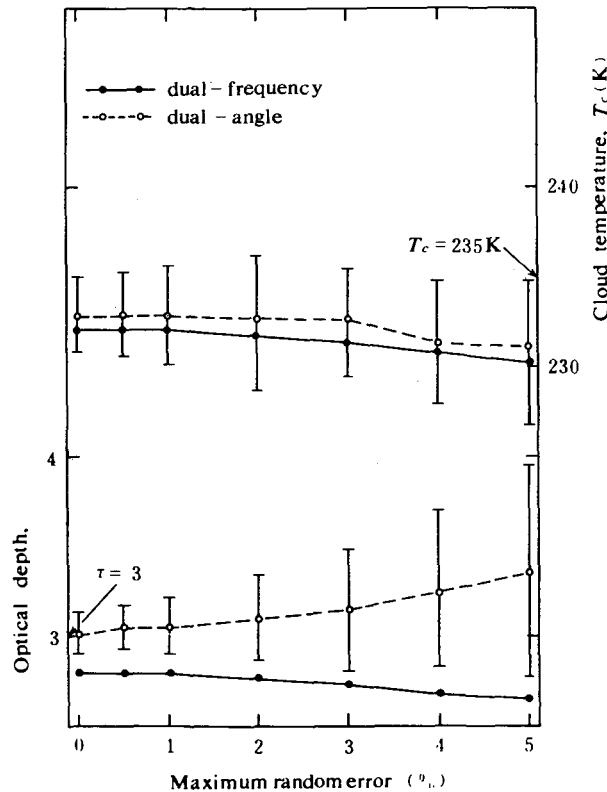

Fig. 7. Same as Fig. 6, except for an intermediate thick cirrus with a cloud temperature of 235 K.

V. CONCLUSIONS

In this paper we have made a number of retrieval experiments involving the cirrus optical depth and temperature utilizing two window channels in the 3.7 and 10.8 μm of the AVHRR on board the NOAA 7 satellite. These retrieval experiments are based on the forward radiative transfer parameterization when high, nonblack cirri are present in the field-of-view of the radiometer.

In forward radiative transfer analyses, we first find that atmospheric attenuations in the zenith direction for the 3.7 and 10.8 μm channels are approximately the same. The maximum difference is less than 0.3 K for a total precipitable water of 6 g cm^{-2} corresponding to a rather moist atmosphere. Also, the difference in the atmospheric attenuation for the 3.7 μm channel between different emergent angles, less than 50^0 with respect to the zenith, is within about 0.2 K. Moreover, we find that the directional cloud emissivity depends only on the cloud optical depth and that a second-order polynomial can be utilized to correlate empirically these two parameters.

On the other hand, the cloud attenuation effects using either 3.7 and 10.8 μm channels or two emergent angles for either channel are appreciable. Thus, by virtue of the statistical relationship between the cloud attenuation and the cloud optical depth, the latter may be inferred from the observed brightness temperature difference utilizing either dual-frequency or dual-scanning angle approach.
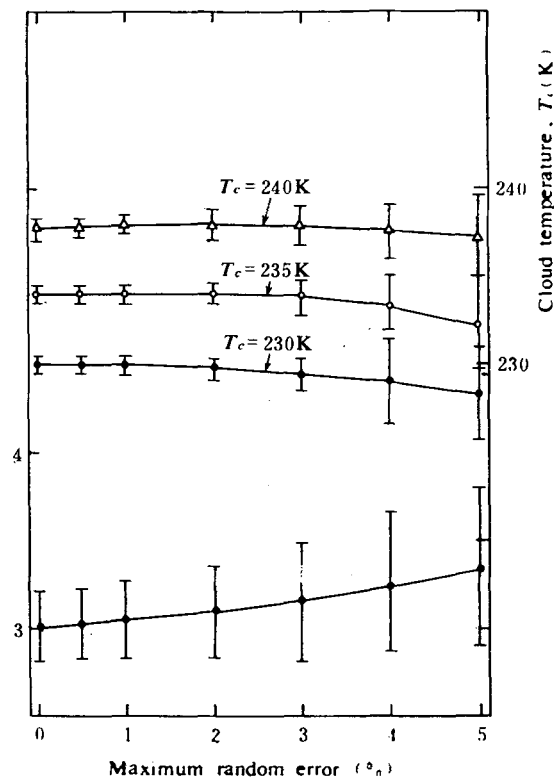
Fig. 8. Retrieval results involving an intermediate thick cirrus with three different temperatures of 230, 235, and 240 K using a combined dual-frequency and dual-scanning angle approach.

In addition, we also clearly show that the cloud temperature and clear-air brightness temperature may also be retrieved by solving the combined parameterization equations for either dual-frequency or dual-scanning angle technique. Numerical experiments and error analyses reveal that the dual-frequency method is particularly suitable for cases involving optically thin cirri with high degrees of retrieval accuracy. However, a combination of dual-frequency and dual-scanning angle approaches will lead to a substantial improvement on retrieval accuracies for the cloud optical depth and cloud temperature for thicker cirri having optical depths greater than about 3.

It should be noted that the technique presented in this paper is only suitable to the nighttime, because of the contamination of the reflected solar radiation at the 3.7 μm wavelength. An appropriate criterion to identify the existence of the cirrus should be developed before using this method. These are two open problems we attempt to solve in the future.

REFERENCES

[1]   Liou, K.N., J.Appl. Met., 16 (1977), 91 -99.

[2]   Feddes, R.G. & Liou, K.N., J.Appl Met., 17 (1978), 536- 551

[3]   Liou, K.N., et al., Pure Appl. Geophys., 116 (1978), 1007 1029.

[4]   Yeh, H. Y. & Liou, K N., J. Climate and Appl. Met., 22 (1983), 201—213.

[5]   Weinreb, M P. & Hill, M L., NOAA Tech. Rep. NFSS, 80 (1980), 1 —40.

[6]   Huang, R.H.& Liou, K.N., *J. Geophys. Res.*, **88** (1983), 3885- -3895.

[7]   Liou, K.N., *J. Atmos. Sci.*, **31** (1974), 522—-532

[8]   Weickmann, H.K., *Ber. Deut. Wetterd.*, 1949, 6, 1—54.

[9]   Heymsfield, A.J., *J. Atmos. Sci.*, **32** (1975), 798—-808.

[10]   Cai, Q.M. & Liou, K.N., *Appl. Opt.*, **21** (1982), 3569—3581.

[11]   Schaaf, J.W. & Williams, D., *J. Opt. Soc. Amer.*, **63** (1973), 726—732.